39th AIAA/ASME/SAE/ASEE Joint Propulsion Conference and Exhibit
20-23 July 2003, Huntsville, Alabama

AIAA 2003-4496

Modeling Pollutant Emission and Lean Blow Out in Gas Turbine Combustors

S. Menon
School of Aerospace Engineering
Georgia Inst. of Technology
Atlanta, Georgia, USA 30332

39th AIAA/ASME/SAE/ASEE Joint Propulsion Conference 20-23 July 2003 / Huntsville, AL

Modeling Pollutant Emission and Lean Blow Out in Gas Turbine Combustors

S. Menon*
School of Aerospace Engineering
Georgia Inst. of Technology
Atlanta, Georgia, USA 30332

Large-Eddy Simulation (LES) is fast becoming a favorite tool to study transient phenomena in both non-reacting and reacting turbulent flow systems. However, LES can be computationally very expensive and even though it can resolve the large-scale structures accurately, the dynamics at the small-scales still require modeling. Therefore, the introduction and use of LES within the engine design cycle must ensure that the high cost and uncertainties in the subgrid models are not counter-productive. Furthermore, LES models validated in one particular regime (e.g., flamelet) may not be applicable in another regime (e.g., broken reaction zone) and this can be problematic when attempting studies of combustion under varying and/or extreme conditions. It is shown here that prediction of pollutant emission (CO, NO, UHC and Soot) in the very lean limit and Lean Blow Out (LBO) will require a more comprehensive approach that captures the underlying physics of small-scale mixing and finite-rate kinetics in a combustion regime were classical concepts of flame are no longer valid. A methodology that can deal with these issues has been developed and its strengths and limitations are highlighted in this paper.

1 Modeling Constraints in the Lean Limit

The gas turbine engine has been in operation for a long time and many variants of this engine has been developed for both land-based energy production and for propulsion (land, air and/or sea). Engine power output has been scaled from the KW range to the 100+ MW (for power generation) range but in many respect, the key features of the gas turbine has remained the same. The scalability and performance improvements were achieved due to technological development in many diverse areas, such as materials, electronics, manufacturing, etc., in addition to optimization of dynamical systems involving fuel-air mixing and combustion. In spite of these advancement, a fundamental fact in gas turbine engine development is that nearly all breakthroughs in engine design and performance has been due to "experimental" parametric studies and historical experience in the industry. This was acceptable till now since the major design metrics were reduced weight, increased thrust-to-weight ratio, improved pattern factor, increase in component life, etc. Only very recently has fuel efficiency and reduced pollutant (CO, NO, UHC and Soot) emission become major design constraints. Achieving fuel-efficiency and also low pollutant emission in the next generation power and/or propulsion system will require a major revision in the current design strategy due to some unavoidable facts.

Both increased fuel efficiency and reduced emission are intimately related to each other due to the dynamical nature of fuel-air mixing and combustion. For example, decrease in fuel consumption can be achieved by making the fuel-air mixture very lean for certain parts of the performance envelope (e.g., idle, cruise and low-power) without sacrificing high-power performance. However, as the equivalence ratio approaches the lean flammability limit many unwanted dynamics begin to occur. Recent measurements in a full-scale premixed methane-air combustor[1] show that, as the equivalence ratio is decreased and approaches the lean flammability limit, the CO emission first decreases and then, suddenly increases exponentially. Local flame quenching and formation of UHC and soot can also occur in the very lean limit. This phenomenon (which is also observed in liquid- and gaseous-fueled gas turbine combustors) can (in some cases) be followed by, or related to combustion instability during which the flame undergoes rapid oscillations and eventual blows out completely. This process is often called lean-blow out (LBO) and understanding and predicting this phenomenon is now a major research issue. This new focus in this area is motivated by the fact that most current gas turbines operate far from the lean limit to avoid these dynamical effects and as a result, produce unacceptable levels of CO and NO (as per ICAO requirements for the next generation engines).

Reducing the equivalence ratio can decrease NO emission but can increase CO and soot if a critical (minimum) value is crossed. Determining this

*Professor, Associate Fellow, AIAA

minimum value and achieving stable combustion at this limit is fundamental for achieving a fuel-efficient, stable and low-emission gas turbine. Parametric experimental studies are not only expensive but also cannot be used to develop and evaluate new designs (that do not exist) without first understanding the complex coupling between turbulence-chemistry-heat release in the lean limit. RANS approach using a modified flamelet model[2,3,4] has been able to achieve good agreement with experimental data for the pollutant emission in a GE LM6000 premixed system but involved extensive adjustments of the sub models. However, these sub models need not be valid for other premixed combustors (as shown recently[5]) and are definitely inapplicable in spray systems. Therefore, a more comprehensive model is critically needed to address pollutant emission and LBO in all kinds of gas turbine combustors without resorting to ad hoc model adjustment.

In this paper, the issues regarding modeling required in LES for predicting pollutant emission and LBO are discussed with a particular focus on application to realistic gas turbine combustors. In particular, very lean combustion is addressed since it is at this limit where significant reduction in pollutant emission (and decrease in fuel consumption) can be achieved. The issues we discuss here apply equally to premixed and non-premixed (both single and two-phase) combustion systems but the finer details may differ depending upon the operating conditions. Here, for brevity we focus on premixed and partially premixed systems for the ensuing discussion.

2 Simulation of Momentum and Energy Transport

Figure 1 shows a schematic that attempts to characterize the various simulation methods in terms of the methodology used to resolve the turbulent length scales (an equivalent schematic in terms of time scales can also be used) in a typical flow. As shown, classical RANS (for very large T) can resolve only the mean motion at the largest length scale (L), whereas at the other end of the spectrum, DNS resolves all length (and time) scales from the largest energy containing (e.g., integral scale l) to the smallest dissipative (Kolmogorov, η) scale. However, most DNS studies are confined to simple flows and to low Re ($O(10^3)$) flows, and its application to real combustion systems is likely to remain an impossibility.

In-between the two extreme methodologies of RANS and DNS lie the methodologies based on VLES and LES. The key (somewhat subjective) difference between these two approaches is the location of the grid-scale cutoff. In VLES (as defined here), the cutoff is in the energy production range while in LES, the cutoff is in the inertial range of turbulence. Obviously, VLES is computationally more efficient than LES and may be preferred when large-scale (coherent) motion dominates the flow and small-scale dynamics is not important.

For both VLES and LES, characteristics length and velocity scales have to specified for the unresolved field. In VLES, both velocity and the length scales are modeled (e.g., by using the RNG $k-\epsilon$ model). On the other hand, in LES the local grid size ($\overline{\Delta}$) is the characteristic length scale. If the cutoff is in the dissipation range then negligible energy remains unresolved but if the cutoff is in the inertial range then a significant portion of the kinetic energy is unresolved. In the former case, the characteristic velocity scale can be estimated using $\overline{\Delta}$ and the local resolved strain-rate tensor (as in the algebraic eddy viscosity model[6]). However, in the latter case, equilibrium between subgrid turbulent kinetic energy production and dissipation (inherent in the algebraic eddy viscosity model) cannot exist. As a result, the velocity scale must adjust to the local non-equilibrium effect. A model based the transport equation for the subgrid kinetic energy[7,8] is an obvious choice (and is also consistent with the VLES limit).

Although the algebraic model has been used in both non-reacting and reacting flows, it is not well suited for high-Re combustion simulations since it assumes the aforementioned equilibrium in the subgrid scales and will require a very high resolution to resolve into the dissipation scale. On the other hand, the subgrid kinetic energy k^{sgs} based model allows for non-equilibrium and resolution of the dissipation scale is not needed. As a result, the grid resolution needed is relatively lower than for the algebraic model. Furthermore, as shown below, k^{sgs} model's ability to provide information on the *local* subgrid turbulence intensity offers an additional advantage for reacting flows and therefore, is considered a preferred model for subgrid closure of momentum transport .

2.1 Compressible or Zero-Mach Number LES?

The Navier-Stokes equations that govern the conservation of mass, momentum, and energy in a fluid can be (and has been) solved in LES using either the full compressible or the zero-Mach number (incompressible) limit. Which form of the equation to employ depends on the problem of interest. The key difference between the two approaches is that the zero-M approach uses a series expansion to eliminate the acoustic field effect from the governing equations and excludes acoustic-vortex-heat release coupling effects. The key advantage is that it allows the effective time step to be based on the larger convective time-scale (as opposed to the acoustic time scale in the compressible approach). On the other hand, it requires a Poisson solution of the pressure equation which can be expensive. Nevertheless, zero-M codes can use larger time-steps and therefore, are computationally cheaper for many applications.

However, zero-M codes usability in problems of interest here is highly questionable for various reasons. Gas turbine combustion occurs in a confined domain with a wide range of velocity scales. For example, flow into a GE LM6000 combustor enters at around 120 m/sec but quickly slows down to 30-50 m/sec due to the sudden expansion. However, further downstream the combustor outflow can be very high due to geometrical convergence. In most gas turbines, outflow can be nearly or completely choked (and the flow velocity can be in the 600-900 m/sec, since the temperature is also very high). In addition to changes in velocity scale, combustion dynamics intimately involves acoustic interaction with the reacting flow system. Note that, even though the frequencies that are excited may be low, coupling can occur over a wide range of frequencies (since radial, azimuthal and longitudinal modes can be excited) and therefore, full coupling of acoustics with the flow is needed to be able to predict combustion instability and acoustic dominated flame effects. To achieve acoustic-flame coupling in zero-M methods, pressure-based solvers have to use a much smaller time-step to capture the acoustic wave propagation. This can be quite expensive if multiple pressure iterations are required to achieve accurate convergence. In contrast, compressible methods does not require pressure solver and evolve acoustics at the appropriate time-scale with full coupling of acoustic-vortex-flame interactions.

Finally, to predict pollutant emission finite-rate kinetics will have to be included and de-coupling chemistry from fluid dynamics by using a very large time-step for the fluid flow can result in significant numerical error. Thus, the large increase in time-step achievable in zero-M method may not be actually enforceable. Note that, even the smaller time-step in the compressible method may be too large when compared to the characteristic time-scale for chemistry. Thus, this issue is a problem for both methods at some level.

It is therefore, considered that for problems highlighted in the previous section for gas turbine combustors, fully compressible methods are preferred. For completeness, the governing LES equations and the subgrid terms are summarized below but more details are given elsewhere.[9] These equations are obtained by spatially Favre filtering the N-S equations[10] such that the flow variables are decomposed into the resolved (supergrid scale) and unresolved (subgrid scale) components:$f = \widetilde{f} + f''$, where the ($\sim$) denotes resolved and ($''$) denotes subgrid quantities. The Favre filtered variable is then defined as: $\widetilde{f} = \overline{\rho f}/\overline{\rho}$, where the over bar represents spatial filtering which is defined as, $\overline{f}(x_i,t) = \int f(x_i^{'},t)G_f(x_i,x_i^{'})dx_i^{'}$. Here, G_f is the filter kernel and the integral extends over the entire domain. Applying the filtering operation (in the present study, a low-pass filter of the computational mesh is used, hence, the characteristic size of this filter is the grid width $\overline{\Delta}$) to the Navier-Stokes equations, the LES equations for mass, momentum, and energy are obtained.

2.2 Compressible flow LES equations

The compressible LES equations are:

$$\frac{\partial \overline{\rho}}{\partial t} + \frac{\partial \overline{\rho}\widetilde{u}_i}{\partial x_i} = 0 \tag{1}$$

$$\frac{\partial \overline{\rho}\widetilde{u}_i}{\partial t} + \frac{\partial}{\partial x_j}[\overline{\rho}\widetilde{u}_i\widetilde{u}_j + \overline{p}\delta_{ij} - \overline{\tau}_{ij} + \tau_{ij}^{sgs}] = 0 \tag{2}$$

$$\frac{\partial \overline{\rho}\widetilde{E}}{\partial t} + \frac{\partial}{\partial x_i}[(\overline{\rho}\widetilde{E} + \overline{p})\widetilde{u}_i + \overline{q}_i - \widetilde{u}_j\overline{\tau}_{ji} + H_i^{sgs} + \sigma_{ij}^{sgs}] = 0 \tag{3}$$

The species equations are not shown here since they are dealt with in the next section. In the above equations, ρ is the mass density, p is the pressure, E is the total energy per unit mass, u_i is the velocity vector, q_i is the heat flux vector, and δ_{ij} is the Kronecker delta. The viscous stress tensor is given by $\tau_{ij} = \mu(\partial u_i/\partial x_j + \partial u_j/\partial x_i) - \frac{2}{3}\mu(\partial u_k/\partial x_k)\delta_{ij}$ where μ is the molecular viscosity coefficient and it is approximated using Sutherland's Law. The pressure is determined from the equation of state for a perfect gas

$$\overline{p} = \overline{\rho}\widetilde{T}\sum_{m=1}^{N} R_m\widetilde{Y_m} + \theta^{sgs} \tag{4}$$

where R_m and Y_m are respectively, the m-th species gas constant and mass fraction. The total energy per unit volume is determined from $\rho E = \rho(e + \frac{1}{2}u_k^2)$ where e is the internal energy per unit mass given by $e = \sum_{m=1}^{N} Y_m h_m - p/\rho$. Here, h_m is the m-th species enthalpy. The caloric equation of state is given by, $h_m = \Delta h_{f,m}^0 + \int_{T^0}^{T} c_{p,m}(T')dT'$ where $\Delta h_{f,m}^0$ is the standard heat of formation at temperature T^0 and $c_{p,m}$ is the m-th species specific heat at constant pressure.

In the LES equations, $\overline{\tau}_{ij}$ and $\overline{q}_i$ are approximated simply in terms of the filtered velocity. The unclosed subgrid terms representing respectively, the subgrid stress tensor, subgrid heat flux, unresolved viscous work and species-temperature correlation are:

$$\begin{cases} \tau_{ij}^{sgs} = \overline{\rho}[\widetilde{u_iu_j} - \widetilde{u}_i\widetilde{u}_j] \\ H_i^{sgs} = \overline{\rho}[\widetilde{Eu_i} - \widetilde{E}\widetilde{u}_i] + [\overline{pu_i} - \overline{p}\widetilde{u}_i] \\ \sigma_i^{sgs} = [\overline{u_j\tau_{ij}} - \widetilde{u}_j\overline{\tau}_{ij}] \\ \theta^{sgs} = \sum m = 1^N R_m[\widetilde{TY_m} - \widetilde{T}\widetilde{Y_m}] \end{cases} \tag{5}$$

2.3 Subgrid closure for momentum transport

In this study, a compressible version of the localized dynamic model[11,12,13] is employed. This model is based on the transport equation for the subgrid kinetic energy:[7,14]

$$\frac{\partial \overline{\rho}k^{sgs}}{\partial t} + \frac{\partial}{\partial x_i}(\overline{\rho}\widetilde{u}_i k^{sgs}) = P^{sgs} - D^{sgs} + \frac{\partial}{\partial x_i}\left(\frac{\overline{\rho}\nu_t}{Pr_t}\frac{\partial k^{sgs}}{\partial x_i}\right) \tag{6}$$

where $k^{sgs} = \frac{1}{2}[\widetilde{u_k^2} - \widetilde{u}_k^2]$ is the subgrid kinetic energy and Pr_t is the turbulent Prandtl number. The terms on the right side of equation (6) represent, respectively, the production, the dissipation, and the transport of the subgrid kinetic energy. The production term is modeled as $P^{sgs} = -\tau_{ij}^{sgs}(\partial\widetilde{u}_i/\partial x_j)$ where the subgrid shear stresses τ_{ij}^{sgs} are evaluated as,

$$\tau_{ij}^{sgs} = -2\overline{\rho}\nu_t(\widetilde{S}_{ij} - \frac{1}{3}\widetilde{S}_{kk}\delta_{ij}) + \frac{2}{3}\overline{\rho}k^{sgs}\delta_{ij}. \quad (7)$$

Here, ν_t is the subgrid eddy viscosity given by $\nu_t = C_\nu(k^{sgs})^{1/2}\overline{\Delta}$ and $\widetilde{S}_{ij} = \frac{1}{2}(\partial\widetilde{u}_i/\partial x_j + \partial\widetilde{u}_j/\partial x_i)$ is the resolved-scale rate-of-strain tensor. The dissipation term is modeled as $D^{sgs} = C_\varepsilon\overline{\rho}(k^{sgs})^{3/2}/\overline{\Delta}$. The two coefficients appearing in the above equations, C_ν and C_ε are determined using a localized dynamic approach. In the following, the localized dynamic k-equation model (denoted hereafter as LDKM) is briefly summarized (more details are given elsewhere[12,13,8]).

As in other dynamic models,[15] the LDKM is also based on the assumption of scale similarity in the inertial subrange. However, LDKM employs the experimentally observed similarity between τ_{ij}^{sgs} and L_{ij} to obtain an *algebraic* closure for the model coefficients. As shown earlier, LDKM avoids the problems encountered in the earlier dynamic formulation (the mathematical inconsistency of Germano *et al.*'s dynamic formulation has been pointed out earlier by[16]). The coefficient evaluation does not result in any numerical instability since the denominator is well defined at the test filter level. Furthermore, the prolonged presence of negative model coefficient (described in[17]) is also avoided since the present model is based on the subgrid kinetic energy (which is never negative). Finally, the dynamically determined C_ε does not vanish in the limit of high Re (a phenomenon that was observed in an earlier dynamic kinetic energy model formulation by[18]). These features of LDKM allows fully localized dynamic evaluation without encountering any numerical instability.

Analysis of results[13] have shown that the LDKM is Galilean-invariant and satisfy the realizability conditions.[19] From a computational standpoint, the cost of the present dynamic procedure is not significant (about the same as Germano *et al.*'s dynamic model) due to its simplicity. The additional computational cost is primarily due to the inclusion of a transport equation for k^{sgs}. For non reacting flows, using reasonable grid resolutions the effects of the subgrid model on the statistical quantities are usually marginal. However, it becomes significant when coarse grids are used as demonstrated in recent studies.[8,20,21] The capability of the LDKM approach in coarse grid LES was also demonstrated in an independent study.[22]

Finally, the subgrid energy flux is approximated as: $H_i^{sgs} = -(\overline{\rho}\nu_t/Pr_t)\,\partial\widetilde{H}/\partial x_i$ where $\widetilde{H}$ is the filtered total enthalpy, $\widetilde{H} = \widetilde{E} + \overline{p}/\overline{\rho}$. The turbulent Prandtl number Pr_t can be obtained using a dynamic approach as described earlier.[23] The subgrid term σ_i^{sgs} is expected to be small[23] and so it is neglected in the present study. The species-temperature correlation θ^{sgs} in the equation of state, equation (4) is also neglected in all conventional LES reported here. However, the the new subgrid approach described below can obtain this correlation directly.

3 Simulation of Reactive Scalar Transport

Since the dynamics in the lean regime is highly transient, it is clear that any numerical effort to simulate this phenomenon must be able to capture the unsteady features in both space and time. At present, large-eddy simulation (LES) appears to be the only viable approach to tackle this problem. This is because, in LES all scales larger than the grid are resolved with spatio-temporal accuracy and thus, the large energy-containing scales (that are defined by the system-level boundary conditions) are simulated rather than modeled (as in RANS).

Eddy viscosity/diffusivity type models for scalar field, on the other hand, are inappropriate since scalar mixing, combustion and heat release all occur at the small scales (which are not resolved in the classical LES approach). In the past, models that are prescribed on the resolved grid have been developed and proposed but their application and validation in complex reacting flows as in a full-scale gas turbine combustors still remains to be demonstrated. Probability density function (pdf) methods are often used with RANS models and their use in LES have also been proposed.[24] However, subgrid pdf simulation can be very expensive and therefore an alternate approach which assumes the pdf in the mixture fraction space has been proposed.[25] However, this method is limited since it requires guessing the pdf shape *a priori* which is problematic when multi-species, finite-rate kinetics (including radical and pollutant kinetics) is to be simulated since the mixture fraction approach is not useful. Furthermore, when dealing with realistic combustors (which have multiple feed systems) the mixture fraction approach has limited (if any) validity.[26]

In this paper, the issues regarding modeling required in LES for predicting pollutant emission and LBO are discussed with a particular focus on application to realistic gas turbine combustors. In particular, very lean combustion is addressed since it is at this limit where significant reduction in pollutant emission (and decrease in fuel consumption) have been achieved. The issues we discuss here apply equally to premixed and non-premixed (both single and two-phase) combustion systems but the finer details may differ depending upon the operating conditions.

Even in premixed lean combustion systems, the finer details can be substantially different depending upon

the local turbulence level. For example, Fig. 2 shows the classical Borghi diagram which shows that depending upon the turbulence intensity u' and characteristic length scale the flame structure can change from the corrugated flamelet to the thin reaction zone to the broken reaction zone regimes. In a typical premixed gas turbine combustion, all these regimes can co-exist. This is illustrated in Fig. 3 which is a diagram proposed earlier[27] to determine the type of flame structure modeled in a typical LES or DNS. It can be seen that most full-scale gas turbine combustors (e.g., GEPS LM6000, DOE-HAT) operate in the thin-reaction zone regime when it is operating in the lean but stable condition (typically, for equivalence ratio of $\phi = 0.5-0.7$). However, when the equivalence ratio is decreased for a given flow condition then the regime quickly shifts to the broken reaction zone regime in which classical premixed flame structure is non-existent. The implication of this will be discussed further below.

Another feature of very lean mixtures is that local flame quenching can occur since such flames have a very low tolerance for high turbulence and flame extinction due to aerodynamic stretch effect can become a dominant feature. Local extinction can lead to combustion instabilities which in turn can lead to global extinction (LBO) and hence, catastrophic failure of the system. Clearly, modeling and predicting very lean premixed combustion accurately will require that these dynamical features (e.g., local flame quenching, combustion instability) must be captured. Since these phenomena occur under conditions where classical flame structure is lost (Fig. 3), it is clear that this type of flow cannot be easily addressed by ad hoc extension of models that work well in the other regimes of premixed combustion.

These issues are also valid in non-premixed single and two-phase combustion system. In such systems, fuel-air mixing is a critical feature that must occur before combustion can take place. However, in a typical spray combustor, liquid fuel is injected through many injectors (both in the pilot and secondary combustion zones) and therefore, premixed, partially premixed and non-premixed flame structures can co-exist or can individually dominate in certain regions of the combustor. When spray systems are also operated in the very lean limit, local-to-global flame extinction and LBO can occur.

3.1 LES scalar model

Scalar fields are affected by three physical processes: advection (due to the velocity field), molecular diffusion and chemical reactions. While the filtered velocity field causes large scale convection of the scalar fields, the subgrid velocity fluctuations lead to fine-scale mixing. Furthermore, molecular diffusion and reaction processes are also small-scale phenomena and hence, are affected strongly by the fine-scale mixing. Scalar subgrid model must take into account all these small-scale processes. Such a model is described in this paper.

The scalar conservation equations can also be filtered (as done for the momentum and energy equations) to obtain the LES resolved equations. These equations are discussed below, although, in the present study, a new approach is employed to circumvent some of the problems encountered while attempting closure of this equation. On applying the LES filter, the LES-resolved equations can be derived as:

$$\frac{\partial \overline{\rho}\widetilde{Y_m}}{\partial t} + \frac{\partial}{\partial x_i}[\overline{\rho}\widetilde{Y_m}(\widetilde{u}_i + V_{i,m})] + \frac{\partial Y^{sgs}_{i,m}}{\partial x_i} = \overline{\dot{\omega_m}} \quad (8)$$

Here, $V_{i,m}$ and $\dot{\omega_m}$ are respectively, the m-th species diffusion velocity (given by Fick's law) and the production/destruction term. Also, $Y^{sgs}_{i,m} = \overline{\rho}(\widetilde{Y_m u_i} - \widetilde{Y_m}\widetilde{u_i})$ is the subgrid scalar flux term. Both $\overline{\dot{\omega_m}}$ and $Y^{sgs}_{i,m}$ require modeling, and their closure is problematic.

3.2 LES flamelet model

The scalar LES equations described above can be used for both non-premixed and premixed combustion. However, under special considerations, simplifications can be used to reduce the computational effort. In particular, for premixed combustion a computationally very efficient model can be used in the flamelet regime which is often encountered in practical combustion devices. In this regime, the flame thickness (δ_L) is much smaller than η and the characteristic burning time (τ_c) is much smaller than the characteristic flow time (τ_t). As a result, the flame structure remains laminar and the flame is a thin front propagating at a speed dictated by the mixture properties, which is wrinkled and convected by the flow.

Numerous regimes diagrams for premixed combustion have been proposed.[28,29] A combustion diagram for LES of turbulent premixed combustion proposed by Pitsch[27] (Fig. 3) can be used to highlight the range of applicability of the flamelet type models. In the corrugated flamelet and the wrinkled flamelet regimes the flame thickness is smaller than the Kolmogorov scale (Ka<1) and flame speed enhancement is a result of surface wrinkling due to turbulence. If turbulent eddies are able to penetrate the flame preheat zone but not into the reaction zone (1<Ka<100), then in this thin-reaction-zone regime flame speed enhancement is via turbulent transport of heat and radicals into the preheat zone and the thickening of the preheat zone. However, even in this regime, the flamelet model can be employed since the reaction zone is still smaller that smallest scale of turbulence.

A model equation that describes the propagation of a thin flame by convective transport and normal burning (self propagation by Huygens' principle), is

the G-equation:[30]

$$\frac{\partial \rho G}{\partial t} + \frac{\partial \rho u_i G}{\partial x_i} = -\rho S_L |\nabla G| \tag{9}$$

where $G(\mathbf{x}, t)$ is a progress variable that defines the location of the flame and S_L is the local un-stretched laminar flame speed. In the flow field, G is prescribed in the range [0,1] with a value of unity in the unburned region and zero in the burnt region with the flame identified by a fixed value of $0 < G_o < 1$. Therefore, equation (9) describes the kinematic balance between convection of a level surface, defined as $G = G_o$, by the fluid velocity and normal propagation at a speed S_L. In this flame model, the flame structure is effectively ignored since only the propagating surface is modeled. As a result, the details on the reaction rates and species diffusion can be ignored.

Applying the LES filtering on this equation leads to:

$$\frac{\partial \bar{\rho}\widetilde{G}}{\partial t} + \frac{\partial}{\partial x_i}\left(\bar{\rho}\widetilde{u_i}\widetilde{G}\right) = -\frac{\partial}{\partial x_i}\bar{\rho}\left(\widetilde{u_i G} - \widetilde{u_i}\widetilde{G}\right) - \overline{\rho S_L |\nabla G|} \tag{10}$$

The subgrid convection term is modeled using a gradient assumption that incorporates the effect of the curvature of the flame:[26] $\frac{\partial}{\partial x_i}\left(\widetilde{u_i G} - \widetilde{u_i}\widetilde{G}\right) = \bar{\rho} D_T \widetilde{\kappa} |\nabla \widetilde{G}|$ where $\widetilde{\kappa}$ is the flame curvature defined as $\widetilde{\kappa} = \nabla \mathbf{n} = \nabla(-\nabla\widetilde{G}/|\nabla\widetilde{G}|)$, ($\mathbf{n}$ is the unit normal vector oriented in the direction of flame propagation). The flame front propagation term $\overline{\rho S_L |\nabla G|}$ is modeled as $\bar{\rho} S_F |\nabla \widetilde{G}|$ where S_F is the flame speed propagation. S_F depends upon the combustion regime and has to be modeled. For laminar flow, $S_F = S_L$, for turbulent flows $S_F = S_T$. The model developed by Pocheau:[31] $S_T = S_L(1 + 20.0(U'/S_L)^2)^{0.5}$ has been combined with models to account for the effect of flame stretch in the thin reaction zone regime.[9]

The LES G-equation must be solved along with the LES equations since G is coupled with the thermodynamic variables through the filtered internal energy $\widetilde{e} = c_v\widetilde{T} + \Delta h_f \widetilde{G} H(G - G_0)$. Here, $\Delta h_f = c_p(T_p - T_f)$ is the heat of formation and T_p, T_f are the product and fuel temperatures, respectively, and $H(G - G_0)$ is a Heavy-side function of G. Thus, heat release occurs in a "thin" zone around G_0 even if $\widetilde{G}$ is diffused due to numerics.

Other models have also been developed for the flamelet regime based on the flame surface density concept through a priori analysis of experimental[32] and DNS[33] data. Although recent progress has been encouraging,[32,33] this subgrid model, to the extent of our knowledge, stills remains unimplemented in a LES for a full-scale gas turbine combustor .

A final point to note is that the flame-speed closure described above requires the knowledge of the subgrid turbulence intensity u'. This field is naturally available when the k^{sgs} subgrid model (LDKM) is employed. In contrast, when the algebraic eddy viscosity model is used there is no way to determine u'. This is another advantage of the k^{sgs} model described in this paper.

If the turbulence level is raised even further, the Kolmogorov scale becomes smaller than the reaction zone (Ka>100) and the smallest turbulent structures have the ability to perturb the reaction process by destroying the reaction zone structure thus promoting flame quenching. In this case, flamelet approach cannot be used. As shown in Fig. 3 this regime is very quickly reached in many of the current operational combustors (e.g., LM 6000, DOE-HAT, DACRS) when the equivalence ratio is decreased. This has significant implication of the present goal of studying emission near the LBO regime.

3.3 Subgrid Scalar Simulation Model

The above closure is a conventional approach in which the G equation is filtered and the unclosed terms are modeled. Also, the flame structure is not actually resolved but is modeled as an infinitely thin surface. As shown above, this approach will fail in regimes of our interest where the reaction is likely to occur in the broken reaction zone regime. Therefore, for this type of combustion a new approach is needed.

It is worth reemphasizing that a simulation model of practical relevance should be able to deal with all the regimes identified in Fig 3 without requiring ad hoc changes. This issue is even more relevant for non-premixed spray combustion.

The approach described here has demonstrated an ability to deal with all types of combustion (premixed to spray) without requiring any model adjustment. It also has shown an ability to deal with pollutant emission and is currently being used to study LBO. We believe that this approach has the potential for addressing the issues raised in the introduction.

In our approach, a subgrid simulation of the scalar field is carried out *within* every LES cell. The scalar fields within the subgrid field evolves due to small-scale processes of molecular diffusion, turbulent stirring and volumetric expansion due to heat release. The subgrid simulation model is a variant of the linear-eddy model (LEM) developed earlier.[34,35,36] The subgrid field is also convected from LES cell to cell due to the large (supergrid) scale velocity field.

The details of this approach (called hereafter LES-LEM) have been reported in the past,[37,38,39,40,41,42,43] we summarize some of the key issues in order to highlight the unique features of this approach.

Consider the following generic form of an un-filtered scalar (temperature, species concentrations) evolution equation:

$$\frac{\partial C}{\partial t} = -\widetilde{u_k}\frac{\partial C}{\partial x_k} - u'_k\frac{\partial C}{\partial x_k} + \frac{\partial}{\partial x_j}\left[D_c\frac{\partial C}{\partial x_j}\right] + w_c \quad (11)$$

Here, $\widetilde{u_k}$ and u'_k are the resolved and unresolved velocity fields, D_c is the diffusion coefficient w_c is a representative source term. In the LES-LEM approach, a two-scale numerical procedure is used which can be formally represented as:

$$\frac{C^* - C^n}{\Delta t_{LES}} = -\widetilde{u_k}\frac{\partial C}{\partial x_k} - (u'_k)^{face}\frac{\partial C}{\partial x_k} \quad (12)$$

$$C^{n+1} - C^* = \int_t^{t+\Delta t_{LES}} \left[u'_k\frac{\partial C}{\partial x_k} + \frac{\partial}{\partial x_j}\left(D_c\frac{\partial C}{\partial x_j}\right) + C_s\right] dt \quad (13)$$

Equation(12) represents the large scale advection of the scalar field by the resolved velocity field and is modeled by transferring fluid volumes between the control volumes on the 3D grid. Also, $(u'_k)^{face}$ in equation (12) represents the component of the subgrid velocity field (on the control volume faces) that causes volume (scalar) transport between LES cells.

The subgrid method for solving the above equations involves (a) conducting LEM model simulations in each of the three-dimensional LES grid cells, (b) transporting the subgrid scalar fields across the LES cell faces to account for large-scale advection and (c) coupling the subgrid heat release effect to the momentum and energy transport via volumetric expansion.

Details of this approach has been given in the cited references above and more details of its application to gas turbine combustors are reported in this conference[44,5]

4 Numerical Approach

The numerical model employed in all our studies is a fully compressible finite-volume solver that is nominally second-order accurate in space and time. A fourth-order accurate scheme is also implemented and typically, the fourth-order scheme is turned on after the initial transients to collect data for statistical analysis. The LDKM model is used to obtain the subgrid closure of the momentum transport.

The GLES approach (used for comparison purposes) uses the flamelet model whereas the LES-LEM model employs the subgrid simulation model. For spray combustion, the droplets are tracked using a fourth-order Lagrangian tracking method based on the Stochastic Separated Flow (SSF) model. As detailed elsewhere[45] this approach also uses the LDKM prediction of the subgrid turbulence to include turbulent dispersion of the droplets *within* each of the LES cell. This is another feature that LDKM provides naturally that is absent in classical algebraic eddy viscosity models. Note that spray combustion is not discussed here for brevity.

The time integration is explicit and is constrained by the CFL criteria. However, this code is implemented in parallel using MPI and has been highly optimized and is highly scalable. Therefore, turn around time is reduced by using a large number of processors. Nevertheless, simulation using LES-LEM with finite-rate kinetics can be very expensive. In order to address this issue, we have been exploring the use of In-Situ Adaptive Tabulation (ISAT)[46] and Artificial Neural Network (ANN) to speed up chemistry evaluation within LES-LEM. Past studies[47] shows that ISAT can significantly speed up chemistry evaluation by a factor of 30-50. However, in transient simulations (as in LES) ISAT continues to grow even after statistically stationary state is reached. This is problematic in parallel simulation since dynamic allocation of memory (needed for ISAT) can quickly overwhelm the processor memory and freeze the simulation.

An alternate method based on ANN[48] has been developed which is trained a priori on the ISAT or accessible composition space and then implemented within the LES solver. ISAT or ANN both have the potential ability to drastically reduce the CPU cost of carrying out finite-rate kinetics and their implementation within the LES-LEM is an ongoing effort.

5 Results and Discussion

In the following, we discuss some of the key results obtained in full-scale combustors simulated under realistic conditions.

5.1 Combustion Dynamics in LM 6000

We recently simulated combustion dynamics in a full-scale gas turbine combustor using the conventional GLES approach to investigate the ability of LES to capture combustion instability. The details of this study have been reported elsewhere[49] and only key results are highlighted here. The dump combustor simulated here consists of a straight inlet duct expanding suddenly into the larger combustion zone. The expansion area ratio is 10.25. The inlet and combustor lengths are 1.25 and 5.5 D_0, respectively, where D_0 is the inlet diameter. A converging section is included near the outflow to accelerate the flow as in real combustors, although the outflow is not choked. A grid of $181 \times 73 \times 81$ (axial, radial, azimuthal directions, respectively) is used with clustering in regions of high shear. The computational grid and geometry are shown together in Fig. 4.

A swirling velocity field (with a 7% Gaussian random field) is specified at the inlet. To obtain different levels of swirl, the azimuthal velocity is adjusted while the axial profile is held fixed. The mean inlet mass-flow-rate ($\dot{m}$), temperature, and pressure are 0.435 kg/s, 673 K, and 1.2 MPa, respectively. The Reynolds number based on the inlet center-line axial velocity and inlet diameter is 527,000. The baseline inlet equiv-

alence ratio is 0.52 which corresponds to a laminar flame speed (S_L) of 17.25 (cm/s) and flame temperature (T_f) of 1812.2 (K). The effect of swirl number S is investigated to show changes in inlet flow can drastically impact the flow-combustion interaction.

The pressure fluctuation p' and the flame surface area F_a' response to swirl intensity is shown in Fig. 6. Strong attenuation in p' occurs during transition from jet-like (low swirl) to re-circulating (i.e., with vortex breakdown) type of flow. The reduction in flame pulsation is accompanied by a reduction in p'. A drop in p' by 6.6 dB from $S = 0.56$ to $S = 1.12$ is achieved. The peak frequency for both simulations is approximately 3 kHz with only a small dependence on the initial swirl. Surprisingly, the fluctuating flame surface area increases with higher swirl. However, the average F_a for $S = 1.12$ is approximately 50% less than that for $S = 0.56$. The reduction in flame area is significant since it is directly related to the fuel consumption rate. For the same fuel mass-flow-rate, the higher-swirl condition is able to fully consume the fuel more rapidly due to higher turbulence intensity and lower axial velocity.

A common source of instability in a gas turbine combustor is the interaction between longitudinal pressure oscillations and fuel feed-lines, and this interaction leads to bulk temporal fluctuations in the incoming Φ. Modeling this actual interaction is not attempted in the study; rather, the effect of explicitly including a time variation on Φ has been studied. During this simulation, the inlet Φ is dropped from an elevated value of 0.62 down to the baseline value of 0.52.

As shown in Fig. 6, the pulsating flame evolves in time along with the product temperature field and a probe of the fluctuating normalized pressure ($p'/ < P >$). At the start of the simulation, the equivalence ratio is highest (0.62) and the product temperature is seen to be higher and then quickly decreases as Φ is decreased. The pressure fluctuation level increases as the equivalence ratio is decreases showing onset of instability. The pressure field responds to the inlet equivalence ratio change within 3-4 cycles suggesting a strong coupling between combustion heat release and acoustic oscillation.

5.2 Pollutant Emission in DOE-HAT Combustor

Prediction of CO, NO_x and UHC emission as a function of equivalence ratio is discussed here. The production of these pollutants occur due to a combined effect of chemical kinetics and turbulent fluid dynamical processes. In the following, we discuss the critical issues using a recent study of premixed combustion in a DOE-HAT.[5]

The DOE-HAT combustor is shown in Fig. 7a). In this combustor, the premixed mixture enters the combustor in a swirling manner through a circular slot. The flame is stabilized by the recirculation in the base of the dump and also by the recirculation created by the center body. Figure 7(b) shows the characteristic grid distribution.

The length of the combustion chamber is 0.5 m, its radius is 0.053 m and the inlet is located between 0.0173 m and 0.0314 m from the centerline. The length of the combustor is chosen so that the emissions predictions (which is only available at 0.381 m from the dump plane) can be computed and compared with data.

The inflow characteristics are chosen as given in the earlier DOE-HAT experiment: the fuel is methane (CH_4) and the reactants enter the combustor with a temperature of 700 K, a pressure of 1.378 MPa., and a mean inflow velocity of 68.6 m/s. The flow is swirling and the swirl number is 0.6. The Reynolds number based on the inlet velocity and the diameter of the center-body is 230,000. A random turbulent field is added to the inflow mean velocity and a subgrid turbulence intensity of around 7 percent is used to specify the incoming subgrid kinetic energy. Characteristic based inflow and outflow boundary conditions[50] are employed for all the reported simulations.

5.2.1 Flame Prediction using the Flamelet Model

In this approach we use the GLES approach to track the flame front using the filtered G model described earlier. In this case, the laminar flame speed is obtained using a flamelet library. The turbulent flame speed closure, i.e., $S_T = S_T(u', S_L)$ is obtained using the Pocheau's model described earlier.

5.2.2 Flame Prediction using LES-LEM

The LES-LEM model is used to simulate finite-rate kinetics within the subgrid using a global 1-step model with five species. This 1-step model is used primarily to provide the laminar flame speed S_L within the subgrid domain. Note that, unlike the GLES approach (where a model for S_T is needed), in the LES-LEM approach, the turbulent advection effect on the laminar flame is naturally included and no model is needed. This is an unique advantage of LES-LEM since the assumption of "thin" flame is implicit in the G-equation model and in the model for S_T.

For the LES-LEM study we employ a subgrid resolution of 12 LEM cells within each LES cell in the flame zone. This resolution is not very large and is primarily used here to demonstrate the potential of LES-LEM. On the other hand, even with this resolution some of the eddies below the LES resolution are resolved within the subgrid simulation (a feature absent in GLES). Increase in the LEM resolution can be considered when required. Figure 8 shows that even for very lean system with $\Phi = 0.41$, the flame zone is well resolved (note that, the Kolmogorov scale is smaller than the reaction zone and thus, local flame quenching is expected, as discussed elsewhere[5]).

5.2.3 Pollutant Prediction

CO, NO and UHC are predicted using the same models for both the GLES and LES-LEM approaches. Thus, the only difference in this comparative study is the manner in which the flame is actually resolved (as noted in the above two sections). Details of the models used for predicting these pollutants are given elsewhere[5] and therefore, only briefly summarized here.

CO is formed and/or destroyed by four major mechanisms. All of these mechanisms are modeled in the simulation, and are (i) the formation of CO at the flame front, (ii) the oxidation of CO in the post flame region, (iii) the dissociation of CO_2, and (iv) the formation of CO via oxidation of unburned CH_4.

Two mechanisms related to NO formation are taken into account in the present study: (i) the production of NO at the flame front and (ii) the production of nitric monoxide due to the Zeldovich mechanism in the post flame region.

If the flame front is partially quenched (mainly due to aerodynamic stretch), pockets of unburnt methane, or UHC, will be released in the post flame region. UHC will oxidize at a rate governed by an Arrhenius-law.[51] In order to predict UHC production at the flame front, the Intermittent Turbulence Net Flame Stretch Model (INFTS[52]) is implemented. Here, only UHC production via aerodynamic stretch flame quenching is modeled.

CO and NO emission are presented on Fig. 9 and Fig. 10, respectively. CO emission predictions are in fairly good agreement with experiments. The right side of the curve (Φ>0.45) correspond to the value of CO mass fraction at equilibrium, and thus, all the CO formed at the flame front and via UHC oxidation is oxidized before reaching the emission probe. The left side of the curve correspond to the kinetic CO.[53] Here, the CO emission is higher than its equilibrium value. Another study[54] suggested that the post flame residence time is too small to allow for the oxidation of the entire amount of CO formed at the flame front, while[55] suggests that a strongly non-uniform equivalence ratio inlet profile is responsible for the knee in the CO curve. The data collected our study[5] suggest that the CO produced in the post flame region via UHC oxidation is the only mechanism able to explain the shape of the curve. Nevertheless, inaccuracy in the UHC prediction model (INFTS is a model for steady state simulation that was adapted for LES here), the extreme simplicity of UHC oxidation model, the absence of heat loss at the combustion chamber wall (decrease in post flame temperature strongly reduces the CO oxidation rate), etc., prevent a better match with experimental data.

No noticeable difference exist between prediction via LES-LEM and GLES methods. Because flame length is significantly different for the two methods,[5] this demonstrates that the amount of CO formed at the flame front cannot explain the CO emission trend.

Finally, the use of LEM in LES is promising in the field of emission prediction because of its ability to simulate flame quenching while the G-equation model cannot be greatly improved to account for flame quenching.

NO emission prediction is in good agreement with experiments for low equivalence ratio but is under-predicted when Φ increases. Because post-flame mechanisms are responsible for a majority of NO emission for Φ>0.5, these results suggest that the NO formation rate in the post-flame region is under-predicted. Other factors, like poor macroscopic fuel unmixedness[56] can increase NO formation at the flame front, and thus, increase the overall NO emission.

5.2.4 Validity in Broken Reaction Zone Regime

As noted earlier, the GLES approach is valid in all regimes but the broken reaction zone. Even in the regions of its validity a turbulent flame speed model is needed, which may or may not be valid. For example, these S_T models fail in the limit of high u'/S_L ratio, i.e., in the range of operation of low equivalence ratio (low S_L). On the other hand, no flame speed model is valid in the broken reaction zone regime. This has been demonstrated theoretically[57] as well as numerically.[58]

The LES-LEM method, on the other hand, is valid in all combustion regimes and does not require any flame speed models since S_L is predicted from the reaction kinetics and S_T (if it exists) is naturally predicted by the subgrid stirring and propagation model in the LEM. In the broken reaction zone the action of stirring can break the flame structure and if the chemical mechanism includes major radicals, stirring events have the capability to quench the flame. This versatility makes of LES-LEM a very powerful method for predicting pollutant emission and LBO. Implementation of ISAT or ANN within LES-LEM will lead to a computationally efficient method to simulate pollutant emission and LBO.

6 Conclusion

This paper summarizes some of the issues related to simulating pollutant emission and LBO in full-scale gas turbine combustors using LES methodology. Many physical issues and modeling constraints have to be considered in order to ensure that the modeling approach can maintain high fidelity in the prediction. Therefore, the introduction and use of LES within the engine design cycle must ensure that the high cost and uncertainties in the subgrid models are not counter-productive. Furthermore, LES models validated in one particular regime (e.g., flamelet) may not be applicable in another regime (e.g., broken reaction zone) and this can be problematic when attempting studies of combustion under varying and/or extreme conditions. It is shown here that prediction of pollutant emission (CO,

NO, UHC) in the very lean limit will require a more comprehensive approach that captures the underlying physics of small-scale mixing and finite-rate kinetics in a combustion regime were classical concepts of flame are no longer valid. The LES-LEM methodology discussed here appears to have all the necessary features to deal with these issues. Some of its strengths and limitations are also highlighted in this paper.

Acknowledgement

This work is supported in part by General Electric Aircraft Engine Company and NASA Glenn Research Center.

References

[1] A. Bhargava, D. W. Kendrick, M. B. Colket, W. A. Sowa, K. H. Casleton, and D. J. Maloney. Pressure effects on no_x and co emission in industrial gas turbines. *Trans. of the ASME*, 2000-GT-8, 2000.

[2] T. J. Held and H. C. Mongia. Application of a partially premixed laminar flamelet model to a low-emission gas turbine combustor. *ASME-98-GT-217*, 1998.

[3] T. J. Held and H. C. Mongia. Emissions modeling of gas turbine combustors using a partially-premixed laminar flamelet model. *AIAA-98-3950*, 1998.

[4] T. J. Held, M. A. Mueller, and H. C. Mongia. A data-driven model for no_x, co and uhc emissions for a dry low emissions gas turbine combustor. *AIAA-2001-3425*, 2001.

[5] G. Eggenspieler and S. Menon. Pollutant prediction in lean combustion system. *AIAA-03-4941*, 2003.

[6] J. Smagorinsky. General circulation experiments with the primitive equations. *Monthly Weather Review*, 91(3):99–164, 1993.

[7] U. Schumann. Subgrid scale model for finite difference simulations of turbulent flows in plane channels and annuli. *Journal of Computational Physics*, 18:376–404, 1975.

[8] W.-W. Kim, S. Menon, and H. C. Mongia. Large-eddy simulation of a gas turbine combustor flow. *Combustion Science and Technology*, 143:25–62, 1999.

[9] W.-W. Kim and S. Menon. Numerical simulations of turbulent premixed flames in the thin-reaction-zones regime. *Combustion Science and Technology*, 160:119–150, 2000.

[10] G. Erlebacher, M. Y. Hussaini, C. G. Speziale, and T. A. Zang. Toward the large-eddy simulation of compressible turbulent flows. *Journal of Fluid Mechanics*, 238:155–185, 1992.

[11] W.-W. Kim and S. Menon. A new dynamic one-equation subgrid-scale model for large-eddy simulations. *AIAA-95-0356*, 1995.

[12] S. Menon and W.-W. Kim. High reynolds number flow simulations using the localized dynamic subgrid-scale model. *AIAA-96-0425*, 1996.

[13] W.-W. Kim and S. Menon. A new incompressible solver for large-eddy simulations. *International Journal of Numerical Fluid Mechanics*, 31:983–1017, 1999.

[14] S. Menon, P.-K. Yeung, and W.-W. Kim. Effect of subgrid models on the computed interscale energy transfer in isotropic turbulence. *Computers and Fluids*, 25(2):165–180, 1996.

[15] M. Germano, U. Piomelli, P. Moin, and W. H. Cabot. A dynamic subgrid-scale eddy viscosity model. *Physics of Fluids A*, 3(11):1760–1765, 1991.

[16] W. H. Cabot and P. Moin. Large eddy simulation of scalar transport with the dynamic subgrid-scale model. In B. Galperin and S. Orszag, editors, *LES of Complex Engineering and Geophysical Flows*, pages 141–158. Cambridge University Press, 1993.

[17] T. S. Lund, S. Ghosal, and P. Moin. Numerical experiments with highly-variable eddy viscosity models. In U. Piomelli and S. Ragab, editors, *Engineering Applications of Large Eddy Simulations*, volume 162 of *FED*, pages 7–11. ASME, 1993.

[18] V. C. Wong. A proposed statistical-dynamic closure method for the linear or nonlinear subgrid-scale stresses. *Physics of Fluids A*, 4(5):1080–1082, 1992.

[19] U. Schumann. Realizability of reynolds-stress turbulence models. *Physics of Fluids*, 20(5):721–725, 1977.

[20] W.-W. Kim and S. Menon. Les of turbulent fuel/air mixing in a swirling combustor. *AIAA-99-0200*, 1999.

[21] W.-W. Kim and S. Menon. Numerical modeling of fuel/air mixing in a dry low-emission premixer. Second AFOSR International Conference on DNS and LES, Rutgers University, June 7-9, 1999, 1999.

[22] C. Fureby, G. Tabor, H. G. Weller, and A. D. Gosman. A comparative study of subgrid scale models in homogeneous isotropic turbulence. *Physics of Fluids*, 9(5):1416–1429, 1997.

[23] C. C. Nelson and S. Menon. Unsteady simulations of compressible spatial mixing layers. *AIAA-98-0786*, 1998.

[24] F. Gao and E.E. O'Brien. A large eddy simulation scheme for turbulent reacting flows. *The Physics of Fluids*, 5(6):1282–1284, 1993.

[25] A. W. Cook and J. J. Riley. Subgrid-scale modeling for turbulent reacting flows. *Combustion and Flame*, 112:593–606, 1998.

[26] N. Peters. *Turbulent Combustion*. Cambridge Monographs on Mechanics, 2000.

[27] H. Pitsch and L. Duchamp De Lageneste. Large-eddy simulation of premixed turbulent combustion using a level-set approach. *Twenty-Ninth Symposium (International) on Combustion*, pages 2001–2008, 2002.

[28] N. Peters. The turbulent burning velocity for large-scale and small scale turbulence. *Journal of Fluid mechanics*, 384:107–132, 1999.

[29] R. Borghi. On the structure and morphology of turbulent premixed flames. In C. Casci and C. Bruno, editors, *Recent Advances in Aerospace Sciences*, pages 117–138. Plenum Press, 1985.

[30] A. R. Kerstein, Wm. T. Ashurst, and F. A. Williams. The field equation for interface propagation in an unsteady homogeneous flow field. *Physical Review A*, 37:2728–2731, 1988.

[31] A. Pocheau. Scale invariance in turbulent flont propagation. *Physical Review E*, 49:1109–1122, 1994.

[32] D. Veynante, J. Piana, J. M. Duclos, and C. Martel. Experimental analysis of flame surface density models for premixed turbulent combustion. In *Twenty-Sixth Symposium (International) on Combustion*, pages 413–420, Pittsburgh, PA, 1996. The Combustion Institute.

[33] M. Boger, D. Veynante, H. Boughanem, and A. Trouve. Direct numerical simulation analysis of flame surface density concept for large eddy simulation of turbulent premixed combustion. In *Twenty-Seventh Symposium (International) on Combustion*, pages 917–925, Pittsburgh, PA, 1998. The Combustion Institute.

[34] A. R. Kerstein. Linear-eddy model of turbulent transport ii. *Combustion and Flame*, 75:397–413, 1989.

[35] A. R. Kerstein. Linear-eddy model of turbulent transport iii. *Journal of Fluid Mechanics*, 216:411–435, 1990.

[36] A. R. Kerstein. Linear-eddy modeling of turbulent transport. part 6. microstructure of diffusive scalar mixing fields. *Journal of Fluid Mechanics*, 231:361–394, 1991.

[37] S. Menon, P.A. McMurtry, and A. R. Kerstein. A linear eddy mixing model for large eddy simulation of turbulent combustion. In B. Galperin and S. Orszag, editors, *LES of Complex Engineering and Geophysical Flows*. Cambridge University Press, 1993.

[38] S. Menon and W. Calhoon. Subgrid mixing and molecular transport modeling for large-eddy simulations of turbulent reacting flows. *Proceedings of the Combustion Institute*, 26:59–66, 1996.

[39] W. H. Calhoon and S. Menon. Linear-eddy subgrid model for reacting large-eddy simulations: Heat release effects. *AIAA-97-0368*, 1997.

[40] T. M. Smith and S. Menon. Subgrid combustion modeling for premixed turbulent reacting flows. *AIAA-98-0242*, 1998.

[41] V.K. Chakravarthy and S. Menon. Modeling of turbulent premixed flames in the flamelet regime. In *Proceedings of first International Symposium on Turbulent and Shear Flow Phenomena*, pages 189–194. Begel House, 1999.

[42] V.K. Chakravarthy and S. Menon. Large-eddy simulations of turbulent premixed flames in the flamelet regime. *Combustion Science and Technology*, 162:1–48, 2000.

[43] V.K. Chakravarthy and S. Menon. Subgrid modeling of premixed flames in the flamelet regime. *Flow, Turbulance and Combustion*, 2001.

[44] V. Sankaran, I. Porumbel, and S. Menon. Large-eddy simulation of a single-cup gas turbine combustor. *AIAA-03-5083*, 2003.

[45] V. Sankaran and S. Menon. Les of spray combustion in swirling flows. *Journal of Turbulence*, 3, 2002.

[46] S.B. Pope. Computationally efficient implementation of combustion chemistry using in situ adaptive tabulation. *Combustion Theory Modelling*, 1:41–63, 1997.

[47] V. Sankaran and S. Menon. The structure of premixed flame in the thin-reaction-zones regime. *Proceedings of the Combustion Institute*, 28, 2000.

[48] S. Menon. The use and relevance of reacting les on engineering design cycle. In *Direct and Large-Eddy Simulations IV*, pages 509–516. Kluwer Press, 2001.

[49] C. Stone and S. Menon. Open-loop control of combustion instabilities in a model gas turbine combustor. *Journal of Turbulence (to appear)*, 2003.

[50] T. Poinsot, D. Veynante, and S. Candel. Quenching processes and premixed turbulent combustion diagrams. *Journal of Fluid Mechanics*, 228:561–606, 1991.

[51] C. K. Westbrook and F. L. Dryer. Simplified reaction mechanisms for the oxidation of hydrocarbon fuels in flames. *Combustion Science and Technology*, 27:31–43, 1981.

[52] C. Meneveau and T. Poinsot. Stretching and quenching of flamelets in premixed turbulent combustion. *Combustion and Flame*, 86:311–332, 1991.

[53] A. H. Lefebvre. *Gas Turbine Combustion*. Taylor and Francis, second edition, 1999.

[54] D. W. Kendrick, A. Bahrgave, Colket M. B., A. W. Sowa, D. J. Maloney, and K. H. Casleton. Nox scaling characteristics for industrial gas turbine fuel injectors. *ASME-2000-GT-98*, 2000.

[55] S. M. Cannon, B. Zuo, and C. E. Smith. Les predictions of combustor emissions from a practical industrial fuel injector. *ASME-2000-GT-98*, 2003.

[56] T. F. Fric. Effects of fuel-air unmixedness on nox emissions. *Journal of Propulsion and Power*, 9(5):708–713, 1993.

[57] J. M. Duclos, D. Veynante, and T. Poinsot. A comparison of flamelet models for premixed turbulent combustion. *Combustion and Flame*, 95:101–117, 1993.

[58] T.M. Smith and S. Menon. One-dimensional simulations of freely propagating turbulent premixed flames. *Combustion Science and Technology*, 128:99–130, 1996.

[59] B. Bédat and R. K. Cheng. Experimental study of premixed flames in intense isotropic turbulence. *Combustion and Flame*, 100:486–494, 1995.

[60] M.S. Mansour, N. Peters, and Y.C. Chen. Investigation of scalar mixing in the thin reaction zones regime using a simultaneous ch-lif/rayleigh laser technique. *Twenty-Seventh Symposium (International) on Combustion*, pages 767–773, 1998.

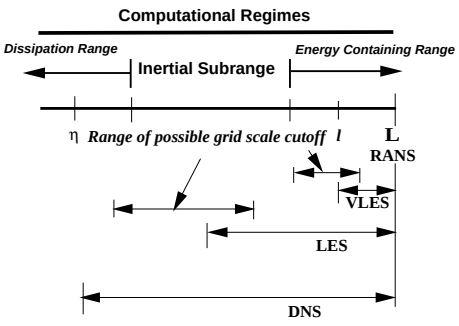

Fig. 1 Characterization of various numerical methods in terms of the turbulent length scales that are resolved.

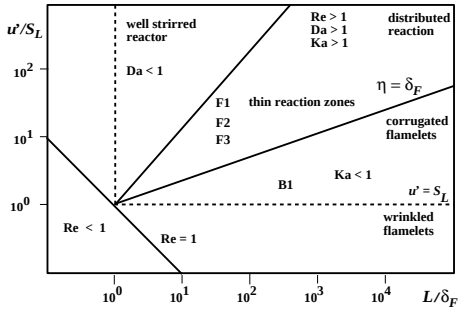

Fig. 2 Diagram of turbulent premixed combustion regimes. The location of F-type and B-type flames are shown.

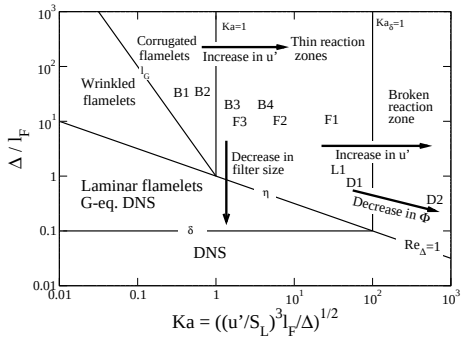

Fig. 3 Combustion regimes for LES of turbulent premixed combustion. B-type[59] and F-type[60] low-Re Laboratory flames, as well as the LM-6000[8] (designated L1) and DOE-HAT (designated by D1 for Φ>0.5 and by D2 for Φ<0.5) gas turbines are shown.

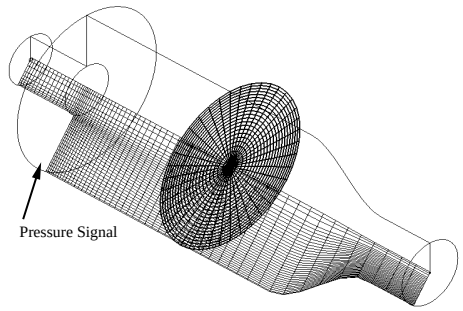

Fig. 4 Geometry and computational grid (181 × 73 × 81) employed for combustion dynamics study.

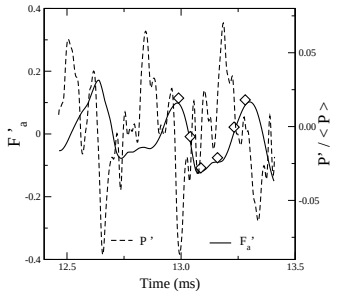

a) $S_0 = 0.56$

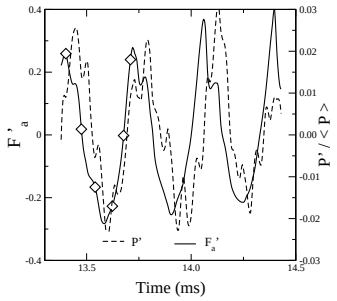

b) $S2$ (S_0= 1.12)

Fig. 5 Fluctuating flame surface area, F'_a, and pressure, p' as a function of time for (a) $S = 0.56$ and (b) $S = 1.12$.

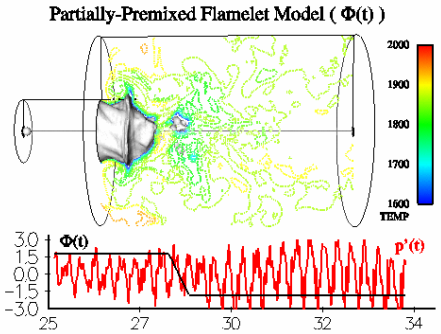

Fig. 6 Product temperature field (contours), flame iso-surface (gray iso-surface), fluctuating pressure ($p'/ < P >$) and inlet equivalence ratio (Φ).

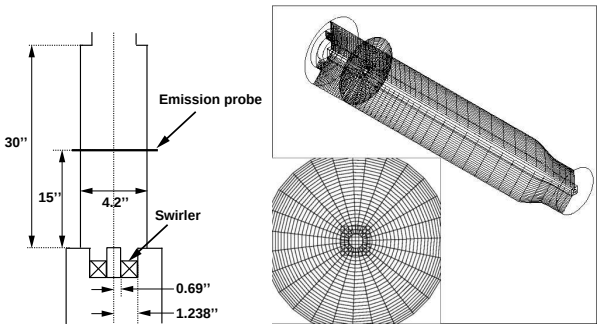

a) Sketch of the DOE-HAT Combustor setup **b)** General view of the 3D computational domain

Fig. 7 Geometry and dimensions of the DOE-HAT combustor and the computational domain.

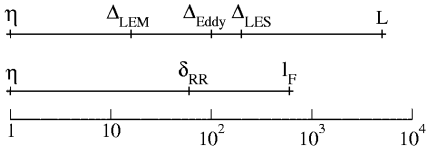

Fig. 8 LES and LEM grid size resolution relative to the flame and reaction zone thicknesses for Φ=0.41.

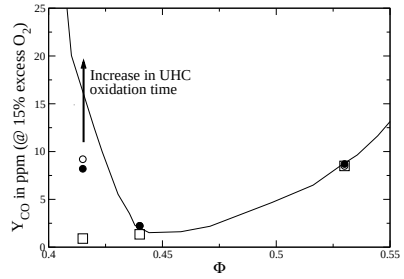

Fig. 9 Experimental and numerical CO emission for different equivalence ratio (—: Experiments, •: LES-LEM with UHC, □: GLES with no UHC model, ○: GLES with UHC model).

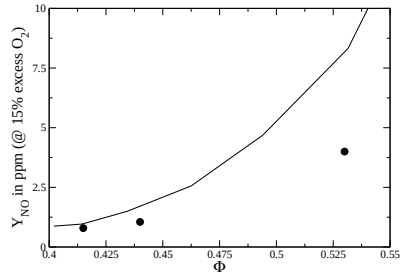

Fig. 10 Experimental and numerical NO emission for different equivalence ratio(— Experiments, •: LES-LEM as well as GLES).